Journal of Molecular Spectroscopy 264 (2010) 10–18

Contents lists available at ScienceDirect

Journal of Molecular Spectroscopy

journal homepage: www.elsevier.com/locate/jms

Organic compounds in the $C_3H_6O_3$ family: Microwave spectrum of cis–cis dimethyl carbonate

F.J. Lovas [a,*], D.F. Plusquellic [a], S.L. Widicus Weaver [b], B.A. McGuire [b], G.A. Blake [c]

[a] Optical Technology Division, National Institute of Standards and Technology, Gaithersburg, MD 20899-8441, USA
[b] Department of Chemistry, Emory University, 1515 Dickey Dr., Atlanta, GA 30322-2210, USA
[c] Division of Geological and Planetary Science, California Institute of Technology, Pasadena, CA 91125, USA

ARTICLE INFO

Article history:
Received 22 July 2010
In revised form 17 August 2010
Available online 18 September 2010

Keywords:
Ab initio calculation
Dipole moment
Dimethyl carbonate
Microwave spectrum
Rotational spectrum
Structure

ABSTRACT

Geometry optimization calculations on 13 members of the $C_3H_6O_3$ family of organic species have been carried out to determine their relative binding energies. Dimethyl carbonate [$(CH_3)_2CO_3$] is one of the lower energy species in this family, which includes the C_3-sugars 1,3-dihydroxyacetone and glyceraldehyde. The microwave spectrum of dimethyl carbonate has been measured over the frequency range 8.4–25.3 GHz with several pulsed-beam Fourier-transform microwave spectrometers and from 227 GHz to 350 GHz with direct absorption spectrometers. The spectrum of the lowest-energy cis–cis conformer of dimethyl carbonate has been assigned, and ab initio electronic structure calculations of the three possible conformers have been performed. Stark effect measurements were carried out on the cis–cis conformer to provide accurate determinations of the dipole moment components.

1. Introduction

Over the past 10 years, a number of spectroscopic efforts have been reported on simple sugars and sugar alcohols in the laboratory and space. The simplest sugar-related species, glycolaldehyde, was detected in the galactic center cloud Sgr B2(N) by Hollis et al. [1], followed shortly thereafter with the detection of the simplest sugar alcohol, ethylene glycol [2]. The presence of larger sugars, sugar alcohols and sugar acids in interstellar space is suggested by the discovery of these species by Cooper et al. [3] in the Murray meteorite and the Murchison meteorite (which is often used as the standard reference for organic species in exogenic material). Surprisingly, ethylene glycol has also been identified in archival spectra from comet Hale-Bopp [4]. Glycolaldehyde belongs to a family of isomers with empirical formula $C_2H_4O_2$ that contains three other members: acetic acid, methyl formate and ethylenediol. With the exception of ethylenediol, whose microwave spectrum is unknown, the three other members of this family have been observed toward the Sgr B2(N) interstellar cloud with relative abundances of (acetic acid):(glycolaldehyde):(methyl formate) of about 1:4:26 [1].

With an interest in extending both laboratory and astronomical measurements to the C_3-sugars with empirical formula $C_3H_6O_3$, a subset of the authors reported the laboratory spectra of the aldose sugar glyceraldehyde [5] and ketose sugar dihydroxyacetone [5,6]. Subsequent searches for both forms of the sugars toward the interstellar cloud Sgr B2(N) were carried out without a clear detection of either [7–9]. This gives rise to the question "Which is the most likely isomer in the family with empirical formula $C_3H_6O_3$ to be detectable in interstellar clouds?"

Structural isomerism is extensive in interstellar clouds, and the relative abundances of isomers offer clues to the chemical and physical processes at play in these environments. Of the ≈160 interstellar species identified to date, two or more structural isomers have been detected for ≈20% of these species. This percentage is artificially weighted to a low value because a number of classes of detected molecules, such as diatomic molecules, do not have structural isomers. Interstellar chemistry is kinetically-controlled, and the expected abundances of structural isomers should therefore be dependent on their relative formation and destruction rates, rather than their relative energies. However, in 2005, Remijan et al. [10] noted that the higher binding energy of organic cyanides, compared to their isocyanide forms, might be the reason that the cyanide forms were found to be more abundant than the isocyanides in interstellar clouds. Likewise, a recent report on complex organic molecules in interstellar clouds by Lattelais et al. [11] noted that for the 32 species with detected structural isomers, the relative energy of the isomers was highly correlated with their relative abundances in interstellar and circumstellar clouds, with the more energetic isomers being less abundant than the lower energy isomers. Lattelais et al. [11] indicated that the two groups of

* Corresponding author. Fax: +1 301 869 5700.
E-mail address: lovas@nist.gov (F.J. Lovas).

0022-2852/$ - see front matter © 2010 Elsevier Inc. All rights reserved.
doi:10.1016/j.jms.2010.08.006

structural isomers that deviated from this trend were those with empirical formulas $C_2H_4O_2$ and C_4H_3N. The first group contains acetic acid (lowest-energy isomer), methyl formate (most abundant isomer, 72 kJ mol^{-1} above acetic acid), and glycolaldehyde (least abundant isomer, highest energy isomer at 114 kJ mol^{-1} above acetic acid). The second group of isomers identified as deviating from this norm was cyanoallene and methylcyanoacetylene. However, the more recent observations by Snyder et al. [12] show that these two isomers are actually equally abundant, with a methylcyanoacetylene column density of $1.8(1) \times 10^{12}$ cm^{-2}, and a cyanoallene column density of $2.0(5) \times 10^{12}$ cm^{-2} [13]. These values are essentially equal within the observational uncertainties and are in line with the expected values based on the relative energies of the isomers.

Given these trends, the relative abundances of the $C_2H_4O_2$ isomers are a mystery. Unlike the other sets of structural isomers detected in the ISM that form primarily through gas-phase ion-molecule chemistry, grain-surface radical–radical reactions involving the products of methanol and formaldehyde photodissociation have been proposed as the dominant formation mechanisms for the $C_2H_4O_2$ isomers [14]. It may be the case that the ice matrix quenches excess energy during the formation of these species, prohibiting molecular rearrangement to form the more thermodynamically-stable species. Before this theory can be tested, however, more information is needed from both laboratory and observational studies that compare the relative abundances of isomers that form through this type of chemistry.

In light of these trends and the puzzling mystery of the $C_2H_4O_2$ isomers, we have carried out theoretical calculations on 13 isomers in the $C_3H_6O_3$ family. We found – not surprisingly – that the sugars, dihydroxyacetone and glyceraldehyde, were not the lowest-energy isomers, and that several hydroxypropionic acid forms and dimethylcarbonate were substantially lower in energy. Given the relative stability of dimethyl carbonate to its sugar analogs, we also undertook the task of measuring its rotational spectrum, which has not been previously investigated. Details of the spectral studies and the theoretical calculations are given below.

2. Theoretical calculations

Nine structural isomers belonging to the $C_3H_6O_3$ family were originally studied by Widicus Weaver [15] and supplemented here with four additional species. Using the GAUSSIAN 09 Quantum Chemistry Package [16,17] at the Cherry L. Emerson Center for Scientific Computation at Emory University, the geometry of each of the four additional structural isomers of the $C_3H_6O_3$ family was initially optimized using Density-Functional Theory (DFT) calculations at the B3LYP/6-311+G level. Next, to find other stable configurations, each functional group on the molecule was rotated about the single bond, when feasible, to the adjacent atom for a total rotation of 360° in 20° increments. Starting with each of the new stable positions for the functional groups, another DFT calculation (B3LYP/6-311+G) was performed to determine which configuration was the energy minimum Each lowest-energy conformer was then optimized at the MP2 6-311++G(d,p) level [18] to obtain its binding energy and rotational constants. Table 1 lists the total binding energies as well as the rotational constants determined for 13 isomers in the $C_3H_6O_3$ family. The relative energies for these structures are shown schematically in Fig. 1. The corresponding 3D structures are shown in Fig. 2. Interestingly, two acid forms, lactic acid (2-hydroxypropionic acid) and 3-hydroxypropionic acid, are found to be the lowest-energy structural isomers in the $C_3H_6O_3$ family, similar to the $C_2H_4O_2$ family where acetic acid is the lowest-energy isomer. The next higher-energy isomers are hydroxymethyl acetate (22 kJ mol^{-1}) and dimethyl carbonate (55 kJ mol^{-1}), neither of which have been previously studied spectroscopically. These two isomers are substantially lower in energy than the two sugar forms 1,3-dihydroxyacetone and glyceraldehyde (≈105 kJ mol^{-1}). Of these four low-energy isomers, only lactic acid has been thoroughly investigated spectroscopically [19]. The only other isomer which is commercially available is dimethyl carbonate.

Dimethyl carbonate is an asymmetric top molecule with three low-energy conformers. The final ab initio calculations on dimethyl carbonate were carried out at the MP2 level [20] with the augmented correlation consistent triple zeta basis set, aug-cc-pVTZ [21], using the GAUSSIAN 09 Quantum Chemistry Package [16,17]. Each of the conformers of dimethylcarbonate is shown in Fig 3. All geometries were at true energy minima as verified in calculations of the analytical second derivatives. The relative energies of the three conformers with and without zero-point-energy (ZPE) corrections are summarized in Table 2. The predicted rotational constants are also reported in Table 2 and were used to aid the identification of the experimentally observed conformer.

3. Experimental details

The microwave spectrum of the lowest-energy conformer of dimethyl carbonate has been observed over a frequency range from 8.4 GHz to 25.3 GHz using pulsed-beam Fourier-transform microwave spectrometers at NIST and in the millimeter-wave range of 227–350 GHz using direct absorption flow cell spectrometers at

Table 1
Binding energy, relative conformational energy, and rotational constants for the 13 structural isomers in the $C_3H_6O_3$ family.

Molecule	Energy[a] (hartree)	Relative energy (kJ mol^{-1})	*A* (MHz)	*B* (MHz)	*C* (MHz)
Lactic acid[b]	−342.841804	0	5135.2	3349.6	2207.5
3-Hydroxypropanoic acid	−342.840992	2.1	7605.4	2397.7	1974.8
Hydroxymethylacetate	−342.833363	22.2	7604.1	2397.8	1975.1
Dimethyl carbonate	−342.821008	54.6	10360.9	2381.3	1984.9
Methyl glycolate	−342.817231	64.6	9959.1	2206.5	1848.3
Methoxy acetic acid	−342.814270	72.3	7565.8	2382.2	2031.5
2-Hydroxyethyl formate	−342.814045	72.9	11217.8	1810.1	1683.9
1,3-Dihydroxyacetone	−342.802330	104	9654.6	2039.8	1732.4
Glyceraldehyde	−342.801845	105	5485.1	2789.5	2408.6
Methoxymethyl formate	−342.795706	121	8995.7	1967.3	1831.1
Trioxane	−342.781161	159	5293.1	5292.5	2949.7
Peroxypropanoic acid	−342.736787	276	8959.0	2193.3	1884.2
Propylene ozonide	−342.698754	376	7586.1	3490.9	2654.8

[a] MP2/6-311++G(d,p) basis.
[b] Also named 2-hydroxypropanoic acid.

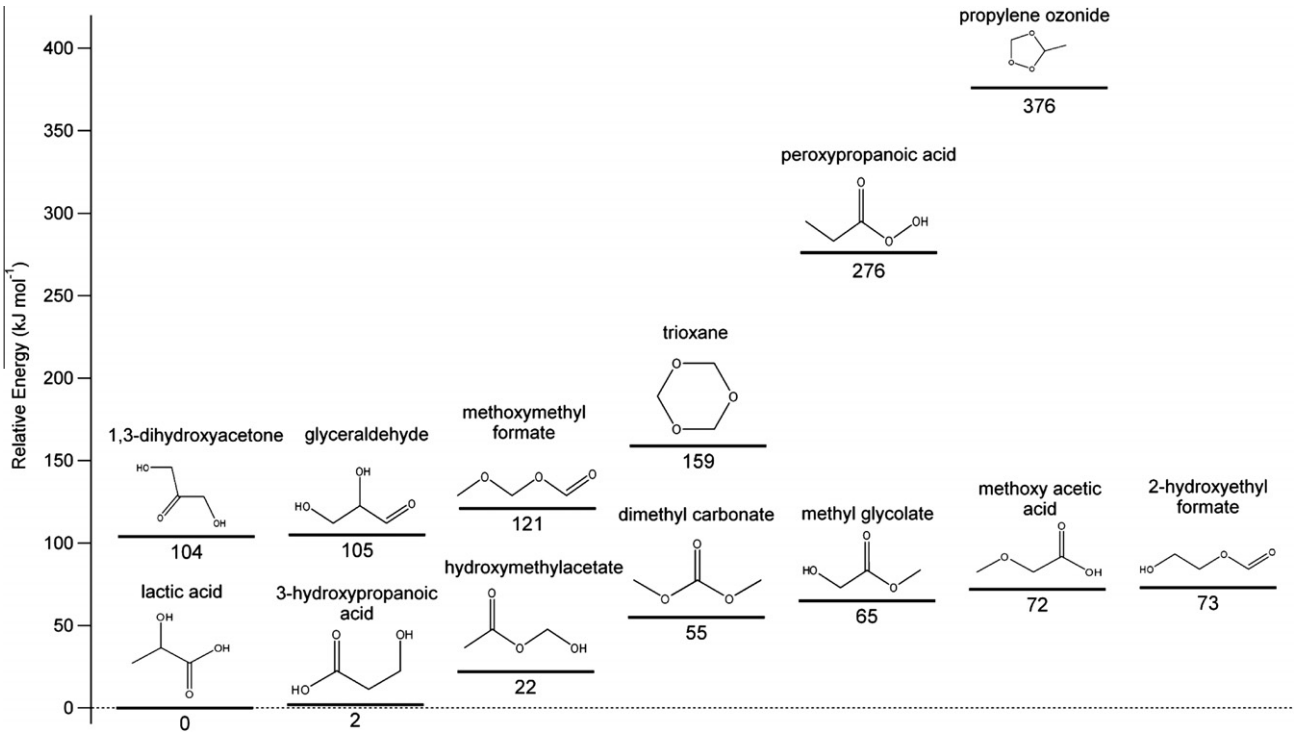

Fig. 1. Relative binding energies for the 13 structural isomers in the $C_3H_6O_3$ family.

Caltech. Additional microwave studies were conducted at Caltech using the original Balle–Flygare spectrometer [22], but the NIST measurements were those used in the analysis presented here.

At NIST, measurements were carried out using a Fabry–Perot cavity, pulsed nozzle Fourier-transform microwave (FTMW) spectrometer of the Balle–Flygare type [22] designed by Lovas and Suenram [23,24]. This design employs a co-axially oriented nozzle [25] and PC-based system for timing, mirror movement, nozzle control, synthesizer tuning and signal processing, and uses the FTMW++ software system designed by Grabow [26]. Under

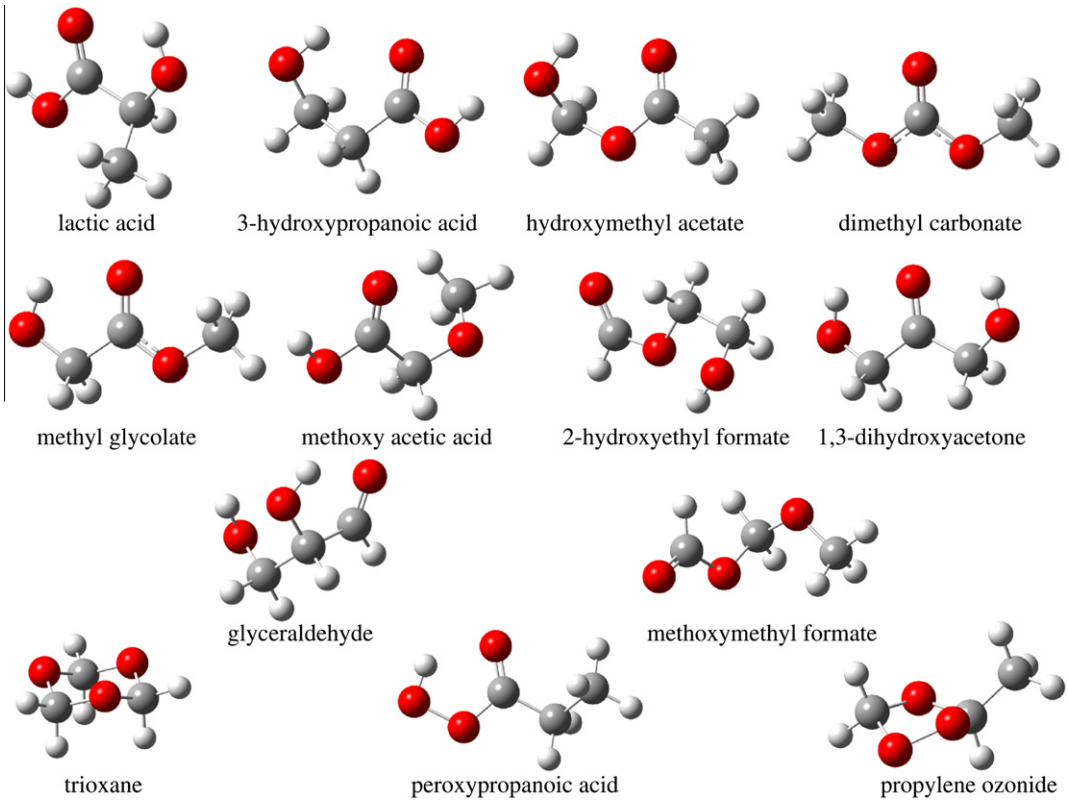

Fig. 2. Structures of the 13 structural isomers in the $C_3H_6O_3$ family.

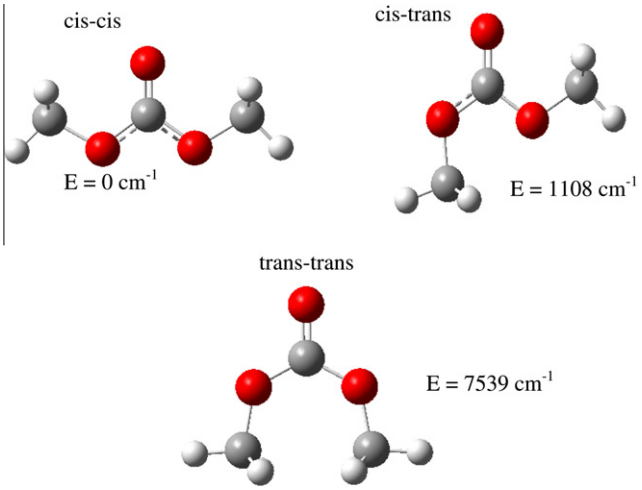

Fig. 3. Structures and relative energies of the three conformers of dimethyl carbonate.

ambient conditions, dimethyl carbonate has a moderate vapor pressure, so that a premixed sample of dimethyl carbonate in rare gas (argon or neon) could be prepared at a 1% by volume ratio. The jet-cooled expansion was produced by pressurizing the pulsed nozzle with this gas mixture at a total pressure of 150 kPa (1.5 bar) and then injecting it into the cavity through a 1 mm diameter nozzle orifice. The expansion was oriented along the axis of the Fabry–Perot cavity and parallel to the microwave field. Molecular transitions, observed as Doppler doublets, had line widths of 5 kHz, and the frequency measurement uncertainties were estimated to be 2.0 kHz in most cases (Type B with $k = 1$ or one standard deviation estimated uncertainty [27]).

For the millimeter-wave measurements, the Caltech direct absorption flow cell spectrometers were employed. These instruments are described in detail elsewhere [28]. Briefly, sample was introduced into a 2-m long glass flow cell via a ball flask connected to the cell. Sample continuously flowed through the cell, and a pressure of about 13 Pa (100 mtorr) was maintained. The millimeter-wave signal was generated by frequency multiplication of the output of a microwave signal generator (Wiltron 6747A-20) via a frequency multiplier chain (including components from Miteq, Spacek, and Virginia Diodes Inc.) [17]. The frequency-modulated output signal was detected with an InSb hot electron bolometer detector and processed with 2f detection using a lock-in amplifier. Computer-automated scans of both increasing and decreasing frequency increments were averaged for all spectra. Since the dimethyl carbonate lines were rather weak and the spectrum quite sparse, multiple (5 or more) up-down sweeps were averaged in small windows around each line. Line measurement uncertainties were estimated to be about 0.1 MHz (Type B with $k = 1$ [27]) due to the step size used and low signal-to-noise ratio as a result of the very small dipole moment. Line widths were typically about 1 MHz.

4. Results and analysis

A survey with the compact FTMW spectrometer at NIST, shown in Fig. 4, was carried out over the frequency range of 9.6–20.5 GHz and used for the initial assignment of the spectrum. Due to the hindered internal rotation of the two methyl groups in dimethyl carbonate, each rotation line appears as a quartet with splittings typically on the order of a few MHz for the lowest K_a transitions. These multiplets are not evident in the low-resolution plot in Fig. 4, and so Fig. 5 shows a high-resolution plot of three $K_a = 1 \leftarrow 0$ R-branch transitions with spin weight labels below each internal rotation component. Note that the spin weights differ only

Table 2
Calculated energies and rotational constants for the three conformers of dimethyl carbonate.

Molecule	Energy[a] (hartree)	Relative energy (kJ mol^{-1})	Relative energy[b] (kJ mol^{-1})	A (MHz)	B (MHz)	C (MHz)
cis–cis Dimethyl carbonate	−342.960485	0	0	10380.4	2389.4	1990.9
cis–trans Dimethyl carbonate	−342.955437	13.29	13.25	6528.4	2999.4	2109.7
trans–trans Dimethyl carbonate	−342.926134	92.1	90.2	4397.0	3926.9	2130.7

[a] MP2 level with aug-cc-pVTZ basis.
[b] Includes zero-point energy corrections.

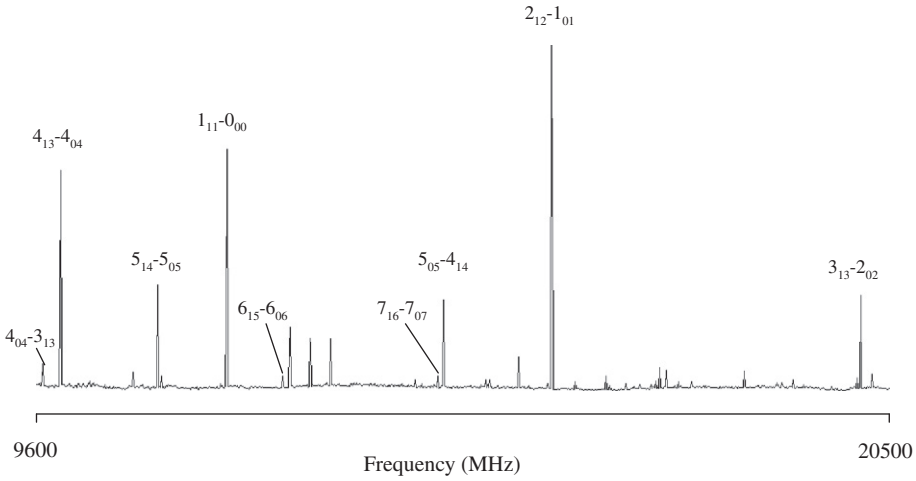

Fig. 4. Survey spectrum of dimethyl carbonate from 9600 MHz to 20 500 MHz.

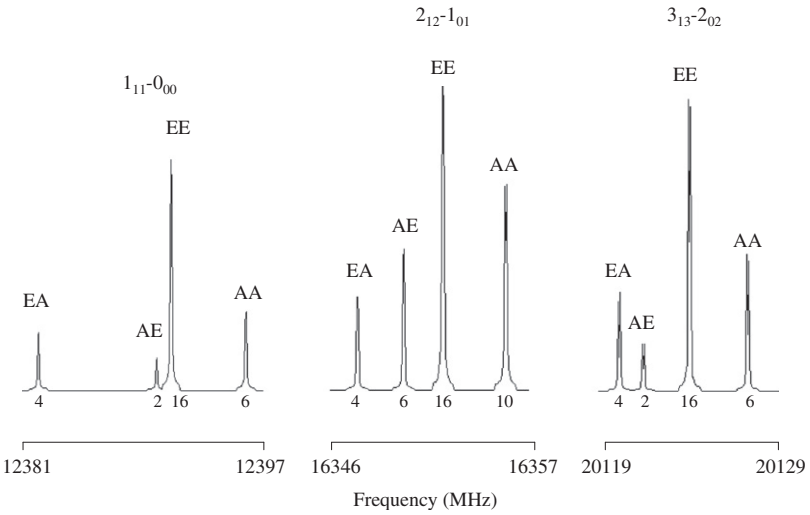

Fig. 5. Example rotational transitions of dimethyl carbonate showing the relative spin weights and observed relative intensities for the internal rotation components which change for K_aK_c values of ee–oo or eo–oe.

for transitions with K_aK_c values of ee/oo compared to those with K_aK_c values of eo/oe for the AE and AA symmetry states. The good agreement between the spin weights and relative intensities of each quartet aided in the assignment of the symmetry state. A total of 19 rotational transitions were assigned over the frequency range of 6.4–25 GHz, each showing the quartet internal rotation structure. These transitions were initially fitted with the Xiam program which treats 2-top internal rotation [29]. Since the Xiam program is limited to rotational quantum number of $J = 20$ or lower, only the FTMW lines could be included in the fit. The Hamiltonian consists of three rotational constants, four of the five centrifugal distortion constants and four internal rotation parameters. The results of this preliminary analysis are shown on the left side of Table 3. The transition quantum numbers, symmetry states, and frequencies are listed in Table 4 along with the fitted observed minus calculated residuals. The 11 kHz standard deviation of the fit is about a factor of five larger than the average uncertainty of the measurements (2 kHz). We were unable to find any additional determinable parameter(s) which improved the fit.

Since we also had observed high-J rotational transitions in the millimeter-wave spectra, listed in Table 5, we employed the Erham program developed by Groner [30] that allows inclusion of rotational quantum numbers up to 120 and a set of Hamiltonian terms similar to those used in the Xiam fit. Due to the large difference in uncertainties and frequencies between the centimeter and millimeter wavelength measurements, the fit was weighted by the inverse of the uncertainties squared. None of the millimeter wavelength measurements exhibited resolved internal rotation and only the degenerate doublets for J'–J'' with $K_a = 1$–0 or 0–1 were observable since these have the largest line strengths. While we initially included only the EE state assignments for these high-J rotational lines, it was not clear if the unresolved internal rotation splitting was symmetric with respect to the EE transition position. Thus, we included all the internal rotation components for each rotational line, i.e., eight transitions at the same frequency. These assignments were weighted by the spin weights, which accounted for two degenerate rotational lines in order to not bias the millimeter wavelength data with respect to the low frequency data set. The final fitted parameters are shown on the right side of Table 3. Tables 4 and 5 show the residuals for this fit, which is clearly an improvement over the Xiam fit for the internal rotation data in Table 4. Table 5 also lists the AA–EE splitting which increases by about 6 kHz per J quantum number. All observed transitions have calculated splitting substantially smaller than the observed line widths of 1–2 MHz. It should be noted that the AE and EA transitions are degenerate in frequency to 1 kHz, and these are split in the opposite direction from the EE lines compared to the AA lines, with splitting values equal to the AA–EE splitting.

Table 3
Calculated rotational and internal rotation parameters.

Parameter	Xiam fitted value[b]	Parameter	Erham fitted value[b]
A (MHz)[a]	10411.707(5)	A (MHz)	10411.707(5)
B (MHz)[a]	2371.5263(9)	B (MHz)	2371.40547(11)
C (MHz)[a]	1980.2513(9)	C (MHz)	1980.37271(7)
Δ_J (kHz)	0.1846[c]	Δ_J (kHz)	0.1846(9)
Δ_{JK} (kHz)	1.41(15)	Δ_{JK} (kHz)	1.448(18)
Δ_K (kHz)	4.76(94)	Δ_K (kHz)	4.70(10)
δ_J (kHz)	0.031(7)	δ_J (kHz)	0.0293(5)
V_3 (cm^{-1})	398.13(20)	V_3 (cm^{-1})	397.19(3)[d]
F_0 (GHz)	157.244(86)	F_0 (GHz)	157.856(20)[d]
θ_1 (°)	25.18(21)°	θ_1 (°)	25.640(11)[d]
θ_2 (°)	154.81(21)°	θ_2 (°)	154.359(11)[d]
		ρ	0.060283(4)
		β (°)	6.239(3)
		ε_{1-1} (MHz)	−0.0149(17)
		ε_{01} (MHz)	−132.383(10)
		$[(B+C)/2]_{10}$ (kHz)	−1.180(27)
N_{lines}	76	N_{lines}	276
Std. dev. (kHz)	11	wt'd. std. dev.	0.59

[a] Derived from fitted values $(B+C)/2 = 2175.8888(6)$ MHz, $A-(B+C)/2 = 8235.8177(46)$ MHz and $(B-C)/2 = 195.6375(6)$ MHz.
[b] Uncertainties from the fit are Type A with coverage factor $k = 2$ (two standard deviations) [26].
[c] Fixed at value from Erham fit.
[d] Derived value.

5. Dipole moment determination

One of the NIST FTMW spectrometers is equipped with a set of 25 cm × 25 cm parallel plates separated by 25 cm [31]. These are positioned along the cavity axis and are centered between the mirrors and the nozzle, which is located perpendicular to the cavity axis. Positive voltage is applied to one plate and an equal negative voltage is applied to the second plate to induce Stark effect shifts in the transitions. The microwave electric field and external electric field are parallel so that $\Delta M = 0$ transitions are observed. The precise Stark plate separation, d, was determined by calibration with

Table 4
Observed FTMW rotation-internal rotation transitions of cis,cis dimethyl carbonate.

Transition	Sym. state (spin wt.)	Measured frequency[a] (MHz)	Xiam obs.-calc. (kHz)	Erham obs.-calc. (kHz)
1(1,0)–1(0,1)	AE/6	8429.2542(20)[a]	−0.1	0.0
1(1,0)–1(0,1)	EE/16	8434.4705(20)	4.1	4.3
1(1,0)–1(0,1)	AA/10	8435.4994(20)	7.2	6.7
1(1,0)–1(0,1)	EA/4	8437.4954(20)	−1.0	0.2
2(1,1)–2(0,2)	AE/2	8834.1880(20)	−3.5	−3.2
2(1,1)–2(0,2)	EA/4	8836.9660(20)	−1.8	−0.6
2(1,1)–2(0,2)	EE/16	8838.0340(20)	2.3	2.4
2(1,1)–2(0,2)	AA/6	8840.4810(20)	−1.2	−2.1
3(1,2)–3(0,3)	AE/6	9467.4133(20)	−0.8	0.1
3(1,2)–3(0,3)	EA/4	9468.7740(20)	−1.8	0.4
3(1,2)–3(0,3)	EE/16	9470.9373(20)	0.8	1.0
3(1,2)–3(0,3)	AA/10	9473.7834(20)	4.5	2.8
4(0,4)–3(1,3)	AA/6	10141.5228(20)	−27.2	−0.3
4(0,4)–3(1,3)	EE/16	10144.7022(20)	−5.1	0.1
4(0,4)–3(1,3)	AE/2	10147.1631(20)	16.0	0.9
4(0,4)–3(1,3)	EA/4	10148.5954(20)	16.8	0.6
4(1,3)–4(0,4)	AE/2	10358.7864(20)	−0.9	0.9
4(1,3)–4(0,4)	EA/4	10359.5717(20)	−3.2	0.6
4(1,3)–4(0,4)	EE/16	10362.2118(20)	1.1	1.1
4(1,3)–4(0,4)	AA/6	10365.2450(20)	3.2	0.1
5(1,4)–5(0,5)	AE/6	11545.2810(20)	−2.6	0.6
5(1,4)–5(0,5)	EA/4	11545.7786(20)	−5.6	−0.1
5(1,4)–5(0,5)	EE/16	11548.6855(20)	0.6	0.3
5(1,4)–5(0,5)	AA/10	11551.8425(20)	4.9	−0.5
1(1,1)–)(0,0)	EA/4	12381.7411(20)	5.3	−0.4
1(1,1)–)(0,0)	AE/2	12389.9950(20)	4.9	0.4
1(1,1)–)(0,0)	EE/16	12391.0134(20)	−1.5	−0.2
1(1,1)–)(0,0)	AA/6	12396.2277(20)	−7.3	−0.5
6(1,5)–6(0,6)	AE/2	13066.8783(20)	−3.7	1.2
6(1,5)–6(0,6)	EA/4	13067.2186(20)	−7.3	0.1
6(1,5)–6(0,6)	EE/16	13070.2993(20)	1.2	0.0
6(1,5)–6(0,6)	AA/6	13073.5529(20)	8.7	−0.1
7(1,6)–7(0,7)	AE/6	14960.2953(20)	−7.5	−0.8
7(1,6)–7(0,7)	EA/4	14960.5514(20)	−9.3	−0.7
7(1,6)–7(0,7)	EE/16	14963.7638(20)	3.4	0.4
7(1,6)–7(0,7)	AA/10	14967.1051(20)	13.9	0.0
5(0,5)–4(1,4)	AA/10	15029.2715(20)	−33.6	−0.3
5(0,5)–4(1,4)	EE/16	15032.1596(20)	−6.3	0.1
5(0,5)–4(1,4)	AE/6	15034.6082(20)	20.3	1.2
5(0,5)–4(1,4)	EA/4	15035.4842(20)	21.7	1.1
2(1,2)–1(0,1)	EA/4	16347.9317(20)	8.7	−0.8
2(1,2)–1(0,1)	AE/6	16350.7385(20)	9.5	0.3
2(1,2)–1(0,1)	EE/16	16353.1405(20)	−4.1	−1.2
2(1,2)–1(0,1)	AA/10	16356.9516(20)	−16.2	−1.9
8(1,7)–8(0,8)	AE/2	17251.3767(100)	−8.8	−1.0
8(1,7)–8(0,8)	EA/4	17251.5849(100)	−9.5	−0.30
8(1,7)–8(0,8)	EE/16	17254.9187(100)	5.8	−0.5
8(1,7)–8(0,8)	AA/6	17258.3580(100)	20.9	−0.2
3(1,3)–2(0,2)	EA/4	20119.9267(20)	13.3	−0.7
3(1,3)–2(0,2)	AE/2	20121.3408(20)	13.6	−0.6
3(1,3)–2(0,2)	EE/16	20124.0632(20)	−4.7	−0.3
3(1,3)–2(0,2)	AA/6	20127.4941(20)	−23.4	−1.4
5(2,3)–5(1,4)	AE/6	22309.4419(20)	−5.4	−2.8
5(2,3)–5(1,4)	EE/16	22324.7501(20)	−1.7	−0.8
5(2,3)–5(1,4)	AA/10	22327.2232(20)	−2.1	0.2
5(2,3)–5(1,4)	EA/4	22334.1374(20)	6.4	1.5
4(2,2)–4(1,3)	AE/2	22980.5275(20)	−2.5	−1.1
4(2,2)–4(1,3)	AA/6	22998.6121(20)	−1.1	0.2
4(2,2)–4(1,3)	EE/16	23003.8674(20)	1.6	0.8
4(2,2)–4(1,3)	EA/4	23029.6966(20)	8.8	3.5
3(2,1)–3(1,2)	AE/6	23606.4677(20)	0.0	0.4
3(2,1)–3(1,2)	AA/10	23624.7567(20)	−2.8	−2.6
3(2,1)–3(1,2)	EE/16	23647.1844(20)	2.2	1.0
3(2,1)–3(1,2)	EA/4	23689.2695(20)	4.4	2.8
4(1,4)–3(0,3)	EA/4	23718.8287(20)	17.4	−1.1
4(1,4)–3(0,3)	AE/6	23719.6902(20)	17.9	−1.1
4(1,4)–3(0,3)	EE/16	23722.4968(20)	−6.3	−0.3
4(1,4)–3(0,3)	AA/10	23725.7355(20)	−30.6	−0.4
2(2,0)–2(1,1)	AE/2	24128.5833(20)	1.5	1.4
2(2,0)–2(1,1)	AA/6	24147.0082(20)	0.7	0.1
2(2,0)–2(1,1)	EE/16	24187.5050(20)	−3.6	−3.5
2(2,0)–2(1,1)	EA/4	24232.9009(20)	−8.5	−5.9

(*continued on next page*)

Table 4 (*continued*)

Transition	Sym. state (spin wt.)	Measured frequency[a] (MHz)	Xiam obs.-calc. (kHz)	Erham obs.-calc. (kHz)
2(2,1)–2(1,2)	EA/4	25183.3701(20)	3.7	0.6
2(2,1)–2(1,2)	EE/16	25247.2970(20)	−0.7	−0.2
2(2,1)–2(1,2)	AE/6	25287.6975(20)	0.7	1.7
2(2,1)–2(1,2)	AA/10	25306.3350(20)	−1.5	−3.4

[a] Estimated uncertainties are Type B coverage factor $k = 1$ [26].

the OCS $J = 1$–0 transition and the known dipole moment of $\mu = 2.3856(10) \times 10^{-30}$ C m (0.71519(3) D) [32].

For cis–cis dimethyl carbonate, the $M = 0$ component of the 1(1,1)–0(0,0) and the $M = 0$ and 1 components of the 2(1,1)–2(0,2) b-type transitions were measured with applied voltages up to 12 kV (positive and negative 6 kV) and frequency shifts up to 0.25 MHz. Because of symmetry, only the μ_b component exists, so a least squares fit of all measurements was used to determine $\mu_b = 0.98(1) \times 10^{-30}$ C m (0.293(3) D), with type A uncertainty for coverage factor $k = 2$ (two standard deviations). This value is quite

Table 5
Observed millimeter-wave rotation-internal rotation transitions of cis,cis dimethyl carbonate.

Transition[a]	Sym. state (spin wt.)	Measured frequency[b] (MHz)	Erham obs.-calc. (kHz)	AA–EE splitting[c] (MHz)
57(*k*,57)–56(*k*,56)	EE/16	227481.663(100)	176	−0.024
58(*k*,58)–57(*k*,57)	EE/16	232437.221(100)	169	−0.018
59(*k*,59)–58(*k*,58)	EE/16	235392.586(100)	144	−0.011
60(*k*,60)–59(*k*,59)	EE/16	239347.718(100)	66	−0.005
64(*k*,64)–63(*k*,63)	EE/16	255166.699(100)	65	0.021
65(*k*,65)–64(*k*,64)	EE/16	259120.953(100)	54	0.027
66(*k*,66)–65(*k*,65)	EE/16	263075.049(100)	83	0.035
68(*k*,68)–67(*k*,67)	EE/16	270982.525(100)	31	0.047
69(*k*,69)–68(*k*,68)	EE/16	274936.064(100)	116	0.054
70(*k*,70)–69(*k*,69)	EE/16	278889.280(100)	88	0.060
71(*k*,71)–70(*k*,70)	EE/16	282842.306(100)	84	0.066
72(*k*,72)–71(*k*,71)	EE/16	286794.999(100)	−36	0.072
73(*k*,73)–72(*k*,72)	EE/16	290747.599(100)	−30	0.079
74(*k*,74)–73(*k*,73)	EE/16	294700.049(100)	49	0.085
75(*k*,75)–74(*k*,74)	EE/16	298652.240(100)	95	0.091
76(*k*,76)–75(*k*,75)	EE/16	302604.130(100)	69	0.097
77(*k*,77)–76(*k*,76)	EE/16	306555.712(100)	−33	0.104
78(*k*,78)–77(*k*,77)	EE/16	310507.201(100)	6	0.110
79(*k*,79)–78(*k*,78)	EE/16	314458.438(100)	32	0.116
82(*k*,82)–81(*k*,81)	EE/16	326310.418(100)	−163	0.134
83(*k*,83)–82(*k*,82)	EE/16	330260.813(100)	3	0.140
84(*k*,84)–83(*k*,83)	EE/16	334210.754(100)	−31	0.147
85(*k*,85)–84(*k*,84)	EE/16	338160.198(100)	−307	0.153
87(*k*,87)–86(*k*,86)	EE/16	346059.198(100)	96	0.165
88(*k*,88)–87(*k*,87)	EE/16	350007.927(100)	−167	0.171

[a] Labels denote either $k = 1$ and 0 or 0 and 1 for the upper and lower states, respectively. Thus, each entry represent two degenerate transitions.
[b] Estimated uncertainties are Type B coverage factor $k = 1$ [26].
[c] The AA and degenerate AE, EA pair are offset symmetrically from the EE transition to within 1 kHz and have equal relative intensities.

Table 6
Observed and calculated parameters for dimethyl carbonate. Calculated values were determined at the MP2/aug-cc-pVTZ level of theory with zero-point energy correction included.

Parameter	Observed[a]	Ab initio cis–cis dimethyl carbonate	Percent difference obs.-calc.	Ab initio cis–trans dimethyl carbonate
A (MHz)	10411.707(5)	10380.4	0.3%	6528.4
B (MHz)	2371.4055(1)	2389.4	−0.8%	2999.4
C (MHz)	1980.3727(1)	1990.9	−0.5%	2109.7
Δ_J (kHz)	0.1846(9)	0.189	−2.4%	0.46
Δ_{JK} (kHz)	1.448(18)	1.38	4.8%	−0.61
Δ_K (kHz)	4.70(10)	4.35	7.4%	5.71
δ_J (kHz)	0.0273(5)	0.031	−10.7%	0.16
V_3 (cm^{-1})	397.19(3)	382.4[b]	3.9%	
F_0 (GHz)	157.856(20)	157.84	0.3%	
θ_1 (°)	25.640(11)°	28.3°	12%	
θ_2 (°)	154.359(11)°	151.7°		
N_{lines}	276			
wt'd. std. dev.	0.59			
Energy (cm^{-1})	0	0.0		1108

[a] Uncertainties from the fit are Type A with coverage factor $k = 2$ (two standard deviations) [26].
[b] The V_3 barrier includes small corrections for zero-point energy differences as described in the text.

Table 7
Comparison of the structural parameters calculated for carbonic acid and dimethyl carbonate.

Parameter	cis–cis Carbonic acid	cis–cis Dimethyl carbonate	cis–trans Carbonic acid	cis–trans Dimethyl carbonate
$r(C_1O_1)$	1.333 Å	1.337 Å	1.354 Å	1.347 Å
$r(C_1O_2)$	1.333 Å		1.336 Å	1.337 Å
$r(C_1{=}O)$	1.203 Å	1.211 Å	1.194 Å	1.205 Å
$r(C_2O_1)$	–	1.436 Å	–	1.438 Å
$r(C_3O_2)$	–	1.436 Å	–	1.436 Å
$\angle HO_1C$	105.7°	–	106.1°	–
$\angle HO_2C$	105.7°	–	108.6°	–
$\angle C_2O_1C$	–	113.3°	–	113.2°
$\angle C_3O_2C$	–	113.3°	–	118.5°
$\angle O_1C{=}O$	125.7°	126.1°	125.2°	125.3°
$\angle O_2C{=}O$	125.7°	126.1°	124.1°	122.8°

consistent with the MP2/aug-cc-pVTZ value of -0.77×10^{-30} C m (-0.23 D). The Stark effect measurements cannot determine the sign of the dipole moment.

6. Discussion

A comparison of the experimentally-determined molecular parameters for cis–cis dimethyl carbonate with those determined from ab initio calculations is shown in Table 6. The rotational and centrifugal distortion constants are in excellent agreement with deviations of less than 1% and up to 10%, respectively. The only parameters easily derived from the internal rotation analysis are the methyl top axis angle relative to the a-principal axis of the molecule, θ_1 (or its complement θ_2) and the V_3 torsional barrier for the two symmetrically equivalent rotors. When the effective methyl top axis is taken to coincide with the O–C(H_3) bond, the angle only agrees to within 22%. However, for an axis defined from the O atom to the center-of-mass of the methyl hydrogens, the angle decreases to 28.3° and F_0 decreases to 157.84 GHz, both of which are in better agreement with the experimental values. The V_3 torsional barrier was calculated by first fully optimizing the double transition state structure defined after rotation of both methyl rotors by 180°. One half of the zero-point corrected energy difference between the equilibrium and top-of-barrier C_{2v} structures was then added to the zero-point energy calculated for the observed V_3 torsional potential resulting in a calculated V_3 barrier of 382.4 cm^{-1}. This value is only 4% lower then the observed value of 398.13(20) cm^{-1}. These results are summarized in Table 6.

Recently, the simplest carbonate molecule, carbonic acid (H_2CO_3), has been observed in the microwave region by Mori et al. [33]. In this case, it was necessary to produce the molecule in a DC discharge of water and carbon dioxide. Due to the small dipole moment of the cis–cis form, only the cis–trans isomer was observed. Since the carbonic acid and dimethyl carbonate species are the first carbonates to be studied with high-resolution rotational spectroscopy, it is interesting to compare their structures derived from ab initio calculations with comparable basis sets. From the values in Table 7, it is evident that substitution of a methyl group has the largest effect on the carbonyl bond length, which increases by 0.008 Å for the cis–cis conformer and 0.011 Å for the cis–trans conformer. The core CO_3 angular geometry does not change significantly. The other large change occurs in the ∠HOC and ∠MeOC angles, which increase about 6° upon methyl group substitution. This may be attributed, at least in part, to steric effects.

In answer to the question posed in the Introduction, "Which is the most likely isomer in the family with empirical formula $C_3H_6O_3$ to be detectable in interstellar clouds?", the most energetically-favored species would be the two hydroxypropanoic acids, which are found to be at the lowest-energy in this group. However, in light of the fact that acetic acid is not the most abundant of the $C_2H_4O_2$ isomers, perhaps the formation mechanisms, destruction mechanisms, or physical mechanisms for release of acids from grain mantles limit the observed abundances of acids in the gas-phase, thus making some of the slightly higher-energy isomers more favorable, e.g., in this case hydroxymethylacetate or dimethyl carbonate. The very small dipole moment of dimethyl carbonate makes it a much less viable candidate for observational detection than hydroxymethylacetate.

Recently, Apponi et al. [34] reported the lack of detection of lactic acid toward Srg B2(N) at 2 mm wavelength with the Arizona Radio Observatory (ARO) 12 m telescope. Their searches realized a column density upper limit of $<9 \times 10^{13}$ cm^{-2} for lactic acid compared to a column density of 7.3×10^{15} cm^{-2} for acetic acid reported by Mehringer et al. [35]. The lower energy form of the C_3 sugar, dihydroxyacetone, was also sought with the ARO 12 m telescope and resulted in a lack of detection with an upper limit column density of $<5 \times 10^{13}$ cm^{-2} [34]. Thus, members of the $C_3H_6O_3$ family are proving to be difficult to observe in the organically rich interstellar cloud Sgr B2(N).

Acknowledgments

The authors gratefully acknowledge P. Groner for the use of his Erham program and some advice on its use. S.L.W.W. and B.A.M. thank M. Heaven for his input on the electronic structure calculations. This work was supported in part by NSF Centers for Chemical Innovation through grant 0847919. The Caltech experimental work and the original computational work were funded in part by the NASA Exobiology and SARA programs, Grant Nos. NAG5-11423 and NAG5-13457. The additional computational work was supported by SLWW's startup funds provided by Emory University.

Appendix A. Supplementary data

The supplementary material can be found online on Science Direct (http://www.sciencedirect.com) and is also available as part of the Ohio State University Molecular Spectroscopy Archives.

Supplementary data associated with this article can be found, in the online version, at doi:10.1016/j.jms.2010.08.006.

References

[1] J.M. Hollis, F.J. Lovas, P.R. Jewell, Astrophys. J. (Lett.) 540 (2000) L107–L110.
[2] J.M. Hollis, F.J. Lovas, P.R. Jewell, L.H. Coudert, Astrophys. J. (Lett.) 571 (2002) L59–L62.
[3] G. Cooper, N. Kimmich, W. Bellsle, J. Sarinanna, K. Brabham, L. Garrel, Nature 414 (2001) 879–883.
[4] J. Crovisier, D. Bockelée-Morvan, N. Biver, P. Colom, D. Despois, D.C. Lis, Astron. Astrophys. 418 (2004) L35–L38.
[5] F.J. Lovas, R.D. Suenram, D.F. Plusquellic, H. Møllendal, J. Mol. Spectrosc. 222 (2003) 263–272.
[6] S.L. Widicus Weaver, R. Braakman, D.R. Kent IV, G.A. Blake, J. Mol. Spectrosc. 224 (2004) 101–106.
[7] J.M. Hollis, P.R. Jewell, F.J. Lovas, A.J. Remijan, H. Møllendal, Astrophys. J. (Lett.) 610 (2004) L21–L24.

[8] S.L. Widicus Weaver, G.A. Blake, Astrophys. J. (Lett.) 624 (2005) L33–L36.
[9] A.J. Apponi, D.T. Halfen, L.M. Ziurys, J.M. Hollis, A.J. Remijan, F.J. Lovas, Astrophys. J. (Lett.) 643 (2006) L29–L32.
[10] A.J. Remijan, J.M. Hollis, F.J. Lovas, D.F. Plusquellic, P.R. Jewell, Astrophys. J. 632 (2005) 333–339.
[11] M. Lattelais, F. Pauzat, Y. Ellinger, C. Ceccarelli, Astrophys. J. (Lett.) 696 (2009) L133–L136.
[12] L.E. Snyder, J.M. Hollis, P.R. Jewell, F.J. Lovas, A.J. Remijan, Astrophys. J. 647 (2006) 412–417.
[13] F.J. Lovas, A.J. Remijan, J.M. Hollis, P.R. Jewell, L.E. Snyder, Astrophys. J. (Lett.) 637 (2006) L37–L40.
[14] R.T. Garrod, S.L. Widicus Weaver, E. Herbst, Astrophys. J. 682 (2008) 283–304.
[15] S.L. Widicus Weaver, Ph.D. Thesis, California Institute of Technology, 2005.
[16] Gaussian 09, Revision A.1, M.J. Frisch, G.W. Trucks, H.B. Schlegel, G.E. Scuseria, M.A. Robb, J.R. Cheeseman, G. Scalmani, V. Barone, B. Mennucci, G.A. Petersson, H. Nakatsuji, M. Caricato, X. Li, H.P. Hratchian, A.F. Izmaylov, J. Bloino, G. Zheng, J.L. Sonnenberg, M. Hada, M. Ehara, K. Toyota, R. Fukuda, J. Hasegawa, M. Ishida, T. Nakajima, Y. Honda, O. Kitao, H. Nakai, T. Vreven, J. A. Montgomery Jr., J.E. Peralta, F. Ogliaro, M. Bearpark, J.J. Heyd, E. Brothers, K.N. Kudin, V.N. Staroverov, R. Kobayashi, J. Normand, K. Raghavachari, A. Rendell, J.C. Burant, S.S. Iyengar, J. Tomasi, M. Cossi, N. Rega, J.M. Millam, M. Klene, J.E. Knox, J.B. Cross, V. Bakken, C. Adamo, J. Jaramillo, R. Gomperts, R.E. Stratmann, O. Yazyev, A.J. Austin, R. Cammi, C. Pomelli, J.W. Ochterski, R.L. Martin, K. Morokuma, V.G. Zakrzewski, G.A. Voth, P. Salvador, J.J. Dannenberg, S. Dapprich, A.D. Daniels, Ö. Farkas, J.B. Foresman, J. V. Ortiz, J. Cioslowski, and D.J. Fox, Gaussian Inc., Wallingford, CT, 2009.
[17] Certain commercial products are identified in this paper in order to specify adequately the experimental or theoretical procedures. In no case does such identification imply recommendation or endorsement by the National Institute of Standards and Technology, nor does it imply that the products are necessarily the best available for the purpose.
[18] A.D. McLean, G.S. Chandler, J. Chem. Phys. 72 (1980) 5639–5648.
[19] L. Pszczółkowski, E. Białkowska-Jaworska, Z. Kisiel, J. Mol. Spectrosc. 234 (2005) 106–112.
[20] C. Möller, M.S. Plesset, Phys. Rev. 46 (1934) 618–622;
M. Head-Grodon, J.A. Pople, M.J. Frisch, Chem. Phys. Lett. 153 (1988) 503–506.
[21] T.H. Dunning Jr., J. Chem. Phys. 90 (1989) 1007–1023;
D.E. Woon, T.H. Dunning Jr., J. Chem. Phys. 98 (1993) 1358–1371.
[22] T.J. Balle, W. Flygare, Rev. Sci. Instrum. 52 (1981) 33–45.
[23] F.J. Lovas, R.D. Suenram, J. Chem. Phys. 87 (1987) 2010–2020.
[24] R.D. Suenram, J.-U. Grabow, A. Zuban, I. Leonov, Rev. Sci. Instrum. 70 (1999) 2127–2135.
[25] J.-U. Grabow, W. Stahl, Z. Naturforsch. A 45 (1990) 1043–1044;
J.-U. Grabow, W. Stahl, H. Dreizler, Rev. Sci. Instrum. 67 (1996) 4072–4084.
[26] J.-U. Grabow, Private communication, 2003; see <http://www.pci.uni-hannover.de/~lgpca/spectroscopy/ftmw/>.
[27] B.N. Taylor, C.E. Kuyatt, NIST Tech. Note 1297 (1994) 1–20. The publication may be downloaded from http://physics.nist.gov/Pubs/guidelines/contents.html. The term Type A refers to statistical uncertainties and Type B to model estimated uncertainties. The coverage factor k value gives the number of standard deviations represented in the uncertainty given.
[28] S.L. Widicus, B.J. Drouin, K.A. Dyl, G.A. Blake, J. Mol. Spectrosc. 217 (2003) 278–281.
[29] H. Hartwig, H. Dreizler, Z. Naturforsch. 51a (1996) 923–932.
[30] P. Groner, J. Chem. Phys. 107 (1997) 4483–4498.
[31] L.H. Coudert, F.J. Lovas, R.D. Suenram, J.T. Hougen, J. Chem. Phys. 87 (1987) 6290–6299.
[32] J.M.L.J. Reinartz, A. Dymanus, Chem. Phys. Lett. 24 (1974) 346–351.
[33] T. Mori, K. Suma, Y. Sumiyoshi, Y. Endo, J. Chem. Phys. 130 (2009) 204308-1–204308-7.
[34] A.J. Apponi, M.A. Brewster, J. Hoy, L.M. Ziurys, in: P.F. Weck, V.H.S. Kwong, F. Salama (Eds.), NASA/CP-2006-214549, 2006, pp. 150–153.
[35] D.M. Mehringer, L.E. Snyder, Y. Miao, F.J. Lovas, Astrophys. J. (Lett.) 480 (1997) L71–L74.